Elastic scattering and breakup reactions of the proton drip-line nucleus ^{8}B on ^{208}Pb at 238 MeV

K. Wang,[1] Y. Y. Yang,[1,2,*] A. M. Moro,[3,4] V. Guimarães,[5] Jin Lei,[6] D. Y. Pang,[7] F. F. Duan,[1] J. L. Lou,[8] J. C. Zamora,[5] J. S. Wang,[9,1,2] Z. Y. Sun,[1] H. J. Ong,[1,2,10] X. Liu,[11] S. W. Xu,[1] J. B. Ma,[1] P. Ma,[1] Z. Bai,[1] Q. Hu,[1] X. X. Xu,[1,2] Z. H. Gao,[1] G. Yang,[1,2] S. Y. Jin,[1,2] Y. H. Zhang,[1,2] X. H. Zhou,[1,2] Z. G. Hu,[1,2] and H. S. Xu[1,2]
(RIBLL Collaboration)

[1]*CAS Key Laboratory of High Precision Nuclear Spectroscopy, Institute of Modern Physics, Chinese Academy of Sciences, Lanzhou 730000, China*
[2]*School of Nuclear Science and Technology, University of Chinese Academy of Sciences, Beijing 100080, China*
[3]*Departamento de FAMN, Universidad de Sevilla, Apartado 1065, 41080 Sevilla, Spain*
[4]*Instituto Interuniversitario Carlos I de Física Teórica y Computacional (iC1), Apartado 1065, 41080 Sevilla, Spain*
[5]*Instituto de Física, Universidade de São Paulo, Rua do Matão, 1371, São Paulo 05508-090, São Paulo, Brazil*
[6]*Istituto Nazionale di Fisica Nucleare, Sezione di Pisa, Largo Pontecorvo 3, 56127 Pisa, Italy*
[7]*School of Physics and Beijing Key Laboratory of Advanced Nuclear Materials and Physics, Beihang University, Beijing 100191, China*
[8]*School of Physics and State Key Laboratory of Nuclear Physics and Technology, Peking University, Beijing 100871, China*
[9]*School of Science, Huzhou University, Huzhou 313000, China*
[10]*Research Center for Nuclear Physics, Osaka University, Ibaraki, Osaka 567-0047, Japan*
[11]*Key Laboratory of Radiation Physics and Technology of the Ministry of Education, Institute of Nuclear Science and Technology, Sichuan University, Chengdu 610064, China*

(Received 25 October 2020; revised 9 December 2020; accepted 13 January 2021; published 3 February 2021)

Elastic scattering and breakup angular distributions of the weakly bound radioactive nucleus ^{8}B on a ^{208}Pb target at an incident energy of 238 MeV, which corresponds to four times the Coulomb barrier, have been measured at the HIRFL-RIBLL facility (Institute of Modern Physics, Lanzhou). The data have been analyzed using the optical model and the continuum discretized coupled channels (CDCC) formalism. The measured and calculated elastic scattering angular distributions do not show any significant Coulomb rainbow suppression. The angular distribution for the breakup reaction was measured for the first time at this energy. The angular distribution of the ^{7}Be fragments could be reproduced considering elastic plus nonelastic breakup contributions, with the former evaluated with the CDCC calculations and the latter with the model of Ichimura, Austern, and Vincent [Phys. Rev. C **32**, 431 (1985)]. The comparison of the breakup cross section of ^{8}B with that of ^{11}Be suggests that the Coulomb and centrifugal barriers encountered by the valence proton may suppress the breakup cross section.

DOI: 10.1103/PhysRevC.103.024606

I. INTRODUCTION

Direct nuclear reactions induced by light weakly bound nuclei, such as ^{6,8}He, ^{11}Li, ^{11}Be, ^{8}B, and others, have been extensively investigated both experimentally and theoretically to study their unusual features. Among the direct reactions, elastic scattering is the simplest yet powerful tool to probe the matter densities, surface diffusenesses, and even cluster structures of these nuclei [1–3]. Elastic scattering is known to be affected by strongly coupled reaction channels, which usually results in an enhancement of the total reaction cross section and a departure from the expected behavior for ordinary nuclei, such as the suppression of the oscillatory pattern in the case of Fresnel scattering. The nature of these channels can be very different depending on the structure of the colliding nuclei. Whereas in the case of stable, well bound nuclei couplings to collective excitations of the projectile and/or target nuclei (such as quadrupole and octupole couplings) play a major role [4–6], in the case of weakly bound nuclei other modes gain relevance, such as transfer and breakup modes, due to the very low binding energies and extended spatial distributions of the valence particles in these nuclei [7]. For ^{11}Li and ^{11}Be the breakup can be considered mainly responsible for the large total reaction cross sections [8–11], while for ^{6,8}He the transfer reaction is mainly responsible for the enhancement of total reaction cross sections [12–16]. Moreover, the large breakup and transfer cross sections for light weakly bound nuclei have a significant impact on other reaction channels such as fusion and elastic scattering [17–19].

For weakly bound nuclei in the proton-rich side, such as ^{8}B, the situation is less clear. With a separation energy of $S_p = 0.136$ MeV, ^{8}B is a proton halo nucleus, which has a cluster configuration of an inert ^{7}Be core and a valence proton occupying the p-wave orbital. The spatial extension and cluster configuration of the ^{8}B nucleus are rather important

*Corresponding author: yangyanyun@impcas.ac.cn

for describing the elastic and breakup reaction channels. The structure of this nucleus is also very important in astrophysics since the radioactive capture ^{7}Be$(p,\gamma)^{8}$B reaction plays a major role in the production of high-energy neutrinos in the standard solar model [20–22]. The first measurement of the ^{8}B matter radius, which yielded a root-mean-square (rms) value of $R_{\rm rms} = 2.38(4)$ fm, was based on the interaction cross sections [23]. This value is actually smaller than the estimate $R_{\rm rms} = 1.23 \times A^{1/3} = 2.46$ fm, expected for ordinary nuclei, based on electron scattering [24]. More recently, the matter radius for ^{8}B was deduced to be $R_{\rm rms} = 2.58(6)$ fm, via the elastic proton scattering on ^{8}B in inverse kinematics at an energy of 0.7 GeV/u [25]. Assuming that ^{8}B is well described by a ^{7}Be core plus a valence proton, this radius was determined to be a combination of core and valence radii as $R^2_{\rm rms} = 7/8 \times R^2_C + 1/8 \times R^2_v$, with $R_C = 2.25$ fm and $R_v = 4.24$ fm. This experiment clearly evidenced a halo structure for this nucleus.

Due to its low binding energy, one would expect a decoupling of the valence proton and a subsequent enhancement of the breakup probability. The actual effect has been found, however, to be much milder than in the case of neutron halo nuclei and weakly dependent on the target nucleus. For the ^{8}B + ^{12}C reaction [26] the effect of the breakup channels was found to be negligible, and no enhancement of total reaction cross section with respect to more bound systems was observed. For ^{8}B + ^{27}Al [27], some enhancement of the total reaction cross section was reported, although the Fresnel peak remained. For the ^{8}B + ^{58}Ni reaction [28,29], the authors find also an enhancement of the total reaction cross section, which was explained as a combined effect of the proton breakup and the reactions induced by the ^{7}Be core, with no indication of proton transfer. Finally, in the recent measurement of ^{8}B + ^{208}Pb at $E_{\rm lab} = 50$ MeV an enormous total reaction cross section was deduced from elastic scattering. Moreover, the Fresnel peak was completely suppressed. However, CDCC (continuum discretized coupled channels) calculations were not able to reproduce these data, a result that was interpreted by the authors as due to the limitations of the description of ^{8}B as an inert ^{7}Be core plus a valence proton in which possible core excitations are ignored [30].

Breakup observables, such as angular distributions of emitted fragments, are even more sensitive to the ^{8}B configuration as compared to the elastic scattering angular distributions. Some measurements of angular distributions for the breakup process have been performed for ^{8}B + ^{58}Ni at 25.75 MeV [31–35]. The inclusion of the proton halo structure of ^{8}B into the calculations is essential to account for the breakup cross section [31]. Further CDCC calculations for the ^{7}Be fragment angular distributions showed that the ^{8}B structure (size) is responsible for the overall scaling of the breakup cross section while the proton-target potentials affect the overall shape by producing an enhancement at backward angles [32,33]. In Ref. [35], the ^{58}Ni(^{8}B, ^{7}Be) breakup angular distributions were compared with CDCC calculations using two different structure models for the ^{8}B nucleus. By scaling the calculated cross sections to reproduce the data, spectroscopic factors and ANC values were determined, yielding for the latter $C^2 = 0.543 \pm 0.027$ fm^{-1}, independently of the choice of the ^{7}Be + p potential model. Angular distribution measurements of the ^{7}Be fragment from ^{8}B breakup on ^{208}Pb have also been performed at deep sub-barrier energies ($\approx$30 MeV) and breakup dominance was observed, which evidenced that the direct reaction channel is dominant at this energy region for halo nuclei on heavy targets [36].

In previous studies, our group reported the elastic scattering data for the ^{8}B + $^{\rm nat}$Pb reactions at energies around three times the Coulomb barrier but without any breakup observables [37,38]. In this case, no strong breakup coupling effect in the angular distributions was reported. This is at variance with the ^{11}Be + ^{208}Pb reaction, where a strong suppression of the Fresnel peak was observed at a similar bombarding energy [39]. This result suggests that the Coulomb and centrifugal barriers experienced by the proton halo may suppress the breakup couplings effects [40,41]. In this paper, we present new results of the ^{8}B-breakup reaction on a ^{208}Pb target at an energy around four times the Coulomb barrier. The angular distribution of the inclusive ^{7}Be fragments was obtained, which is the first measurement of this observable at this energy range. Elastic and nonelastic breakup components have been computed using the CDCC and the model of Ichimura, Austern, and Vincent, respectively, and their sum compared with the measured inclusive cross section. Elastic scattering angular distributions for ^{3}He, ^{7}Be, and ^{8}B are also analyzed to shed light on the reaction dynamics.

II. EXPERIMENT AND DATA ANALYSIS

The experiment was carried out at the National Laboratory of Heavy Ion Research of the Institute of Modern Physics. Secondary ^{7}Be and ^{8}B radioactive beams were produced by fragmentation of a primary 59.7 MeV/u $^{12}C^{6+}$ beam from the Heavy-Ion Research Facility in Lanzhou (HIRFL) on a 2528-μm-thick ^{9}Be production target [42,43]. The primary beam had an average intensity of about 130 e nA. The ^{7}Be and ^{8}B projectile-like fragments were separated by their magnetic rigidity ($B\rho$) and delivered by the Radioactive Ion Beam Line in Lanzhou (RIBLL) [44,45] to the scattering chamber. The average intensities of ^{7}Be and ^{8}B radioactive beams were 6500 and 550 pps, with purities of 57.6% and 4.9%, respectively. A 500-μm-thick aluminum plate was placed at the first momentum-dispersive focal plane (F1) of RIBLL as a degrader. A 317-μm-thick silicon detector (SD) was placed at the fourth focal plane (F4) to measure the energy loss (ΔE) of the fragments for particle identification purpose during the beam tuning, and removed from the beam line during the runs. Two plastic scintillators were placed at the second (F2) and fourth (F4) focal planes of RIBLL as time-of-flight (ToF) detectors. A complete particle identification was enabled using a combination of the time-of-flight, energy loss, and magnetic rigidity.

The sketch of the detector setup is shown in Fig. 1. Two double-sided silicon strip detectors (DSSDs), segmented into 16 horizontal and 16 vertical strips of 3 mm width on each side, were used to provide the precise position and direction of the incident beam particles. The DSSDs, with thicknesses of 87 μm ($\rm Si_A$) and 74 μm ($\rm Si_B$), respectively, were placed 1516 and 714 mm away from the ^{208}Pb target, as indicated in Fig. 1.

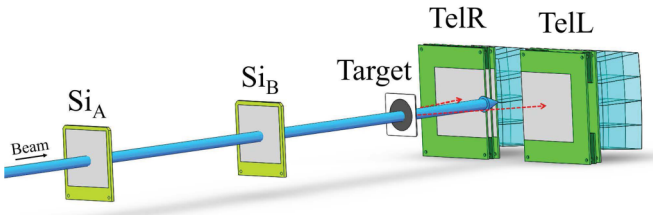

FIG. 1. Sketch of the detector setup. Two DSSDs (Si_A and Si_B) were placed upstream from the target for measuring the beam position. The reaction products were detected with two telescopes, symmetrically mounted around the beam axis, which were composed of two DSSDs, a silicon detector, and an array of CsI(Tl) crystals.

The target consisted of an 8.26-mg/cm^2-thick self-supporting foil, made by the evaporation method. The energies of the secondary beams at the center of the target were about $E_{lab} = 175$ MeV for ^{7}Be and $E_{lab} = 238$ MeV for ^{8}B, with an overall energy resolution of 1.6%. The detection setup was comprised of two ΔE-E telescopes, named TelR and TelL. These detectors were used to measure the reaction products. Each telescope was made up of a thin DSSD, a silicon detector, a thick DSSD, and a CsI(Tl) crystal array. The thin DSSDs (301 and 142 μm thick) with 32 strips on each side and an active area of 64 mm $\times$ 64 mm were used as ΔE detectors in the telescopes. The silicon detectors have thicknesses of (TelR) 1528 and (TelL) 1535 μm and were used to measure the residual energy of the scattered and breakup ^{8}B and ^{7}Be particles. Additionally, thick DSSDs, with 32 strips on each side, a sensitive area of 64 mm $\times$ 64 mm, and thicknesses of 1004 and 998 μm, respectively, were used as the ΔE detectors for measuring protons or any other light particles, while the CsI arrays served as the E detectors. Both CsI arrays were composed of 16 (4 $\times$ 4) CsI(Tl) crystals, and each crystal unit has an active area of 21 mm $\times$ 21 mm. These two telescopes were mounted 272 mm downstream from the target, covering a polar angular range from 3° to 20° in the laboratory frame with a resolution of about 0.4°. The detectors were calibrated with the elastically scattered ^{1}H, ^{4}He, ^{6}Li, ^{7}Be, and ^{8}B particles. During the experiment, the temperature of the detection system was kept at -20 °C with a chilling system that used an alcohol solution for the cooling cycle.

Typical two-dimensional particle identification spectra after the ToF cuts for the ^{7}Be and ^{8}B projectiles on a ^{208}Pb target are shown in Fig. 2. Owing to the superb resolution of ToF signals, which is better than 5 ns (full width at half maximum), the particles in the secondary beam are well separated. It can be seen that no elastic scattered ^{7}Be and ^{8}B beams are mixed with the ^{7}Be products coming from breakup events. The best approach to clearly identify and isolate the elastic breakup component would be to measure the ^{7}Be and proton fragments in coincidence, as performed in Refs. [20,21]. However, due to the limited coverage of the detector setup, the coincidence measurement was not possible and only the ^{7}Be fragment, from the ^{8}B breakup, was measured in the experiment (inclusive breakup).

The angles of elastic scattering and breakup events were determined by considering the incident position and direction

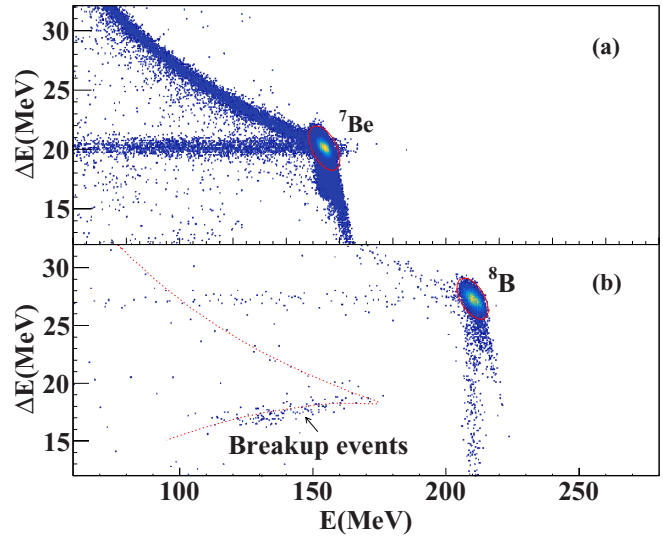

FIG. 2. The calibrated two-dimensional ΔE-E particle identification spectra for the (a) ^{7}Be and (b) ^{8}B projectile nuclei obtained by the TelR telescope, gated by their corresponding ToF. The solid-red-line ellipsoids represent the loci of the elastic scattering events for ^{7}Be and ^{8}B. The dashed line represents the band for ^{7}Be (breakup events), which have the same ToF as ^{8}B but different energy.

of the beam on the target provided by Si_A and Si_B and the hit positions in the telescopes TelR and TelL. Monte Carlo simulations, taking into account the detector geometry and the broad and nonuniform beam profiles on the target, were performed to evaluate the geometrical acceptance, and to determine the absolute differential cross section. With this method, the systematic errors arising from the measurements of the total number of incident beam particles, the target thickness, and the solid angles can be eliminated. More details on the procedure to correct for the the detector misalignment, on the analysis of the contamination from particles scattered by Si_A and Si_B, and on the data normalization are given in Refs. [37,46–49].

III. RESULTS AND DISCUSSION

A global normalization factor [37] for the measured cross sections was extracted from the elastic scattering of a ^{3}He-beam contaminant at forward angles, where the σ/σ_{Ruth} ratio is close to unity. The resulting experimental elastic scattering angular distributions, normalized to the Rutherford scattering cross sections for ^{3}He + ^{208}Pb at $E_{lab} = 55$ MeV, ^{7}Be + ^{208}Pb at $E_{lab} = 175$ MeV, and ^{8}B + ^{208}Pb at $E_{lab} = 238$ MeV are presented in Fig. 3. As for ^{7}Be and ^{8}B, typical Fresnel diffraction patterns can be seen in both distributions, which is consistent with the results obtained for the elastic scattering of ^{8}B + ^{nat}Pb at $E_{lab} = 170$ and 178 MeV reported in Refs. [37,38].

In a first approach, we performed an optical model (OM) analysis to describe the ^{7}Be and ^{8}B elastic scattering data using the code FRESCO [50] with the systematic optical potential proposed by Xu and Pang [51]. This is a global nucleus-nucleus potential constructed with the single-folding model based on the Bruyères Jeukenne-Lejeune-Mahaux

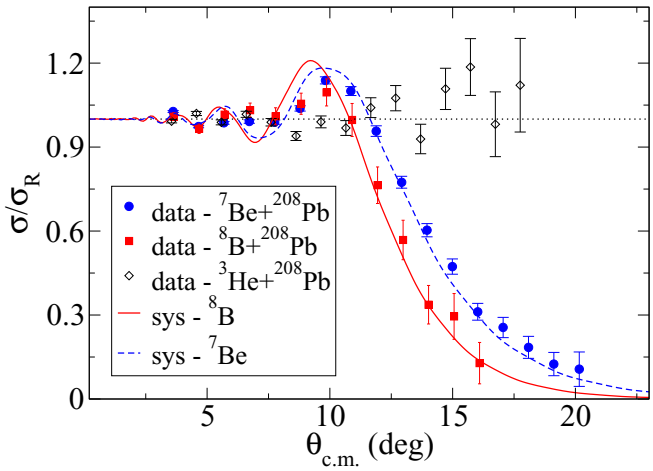

FIG. 3. Elastic scattering angular distributions for $^{3}\mathrm{He}+^{208}\mathrm{Pb}$ at $E_{\mathrm{lab}}=55$ MeV (black empty diamond), $^{7}\mathrm{Be}+^{208}\mathrm{Pb}$ at $E_{\mathrm{lab}}=175$ MeV (blue solid circle), and $^{8}\mathrm{B}+^{208}\mathrm{Pb}$ at $E_{\mathrm{lab}}=238$ MeV (red solid square) and comparisons with OM calculations. Error bars are due to the statistical uncertainty only.

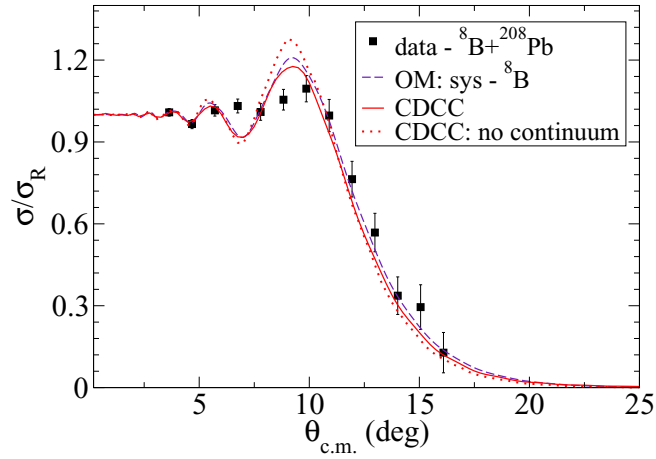

FIG. 4. Elastic scattering angular distributions for the $^{8}\mathrm{B}+^{208}\mathrm{Pb}$ reaction at $E_{\mathrm{lab}}=238$ MeV. Experimental data from the present experiment (black squares) are compared with OM and CDCC calculations. Error bars are statistical only.

(JLMB) semi-microscopic nucleon-nucleus potential and which should take into account reasonable nucleon density distributions of the colliding nuclei [51]. The proton and neutron density distributions for the ^{7}Be, ^{8}B, and ^{208}Pb nuclei were taken from Hartree-Fock calculations with the SkX interaction [52]. The rms radii for the proton distributions were 2.371, 2.537, and 5.441 fm for ^{7}Be, ^{8}B, and ^{208}Pb, respectively. This potential has a simple energy dependence of the potential parameters and it is able to reproduce the angular distributions of elastic scattering and total reaction cross sections for projectiles with atomic masses up to around $A=40$, including both stable and unstable nuclei, and at incident energies up to about 100 MeV/nucleon. The results of the OM calculations are presented in Fig. 3. As seen in the figure, this potential reproduces the data quite well, although it slightly overestimates the data at the Fresnel peak, particularly for $^{8}\mathrm{B}+^{208}\mathrm{Pb}$. The derived total reaction cross sections are 3253 and 3423 mb for $^{7}\mathrm{Be}+^{208}\mathrm{Pb}$ and $^{8}\mathrm{B}+^{208}\mathrm{Pb}$, respectively, corresponding to almost the same reduced cross sections [53], namely, $\sigma_{\mathrm{reduced}}=\sigma_{\mathrm{total}}/(A_{\mathrm{p}}^{1/3}+A_{\mathrm{t}}^{1/3})^{2}=52.95$ and 54.50 mb for ^{7}Be and ^{8}B projectiles, respectively.

To explicitly investigate the importance of the breakup channel and its influence on the elastic scattering angular distribution for the $^{8}\mathrm{B}+^{208}\mathrm{Pb}$ reaction, we have compared the measured data with CDCC calculations. The $^{8}\mathrm{B}+^{208}\mathrm{Pb}$ reaction was described using a standard three-body model in which the ^{8}B projectile is treated as an inert ^{7}Be core plus a valence proton ($^{8}\mathrm{B}\rightarrow{}^{7}\mathrm{Be}+p$). For simplicity, the spin of the ^{7}Be core was ignored.

The p-^{7}Be interaction, required to generate the ^{8}B ground and continuum states, consisted of central and spin-orbit terms with standard Woods-Saxon forms and with the parameters $R_0=2.391$ fm and $a_0=0.52$ fm, adopted from Ref. [54]. For the spin-orbit part, the depth was fixed to $V_{so}=4.898$ MeV whereas for the central part it was adjusted to give the experimental proton separation energy for the ground state of ^{8}B ($S_p=0.136$ MeV). The ground-state wave function obtained with this potential has an ANC value of $C^2=0.53$ fm^{-1}, which is within the range of values extracted from different reactions [35,55–59] and microscopic calculations [60–62]. For continuum states, the same $p+{}^{7}$Be potential was employed. The continuum was discretized using the pseudostate (PS) method, which consists of diagonalizing the projectile Hamiltonian in a basis of square-integrable functions. In this work, we used the transformed harmonic oscillator (THO) basis, which is obtained by application of a local scale transformation (LST) to the conventional HO basis. In particular, we used the analytical LST proposed in Refs. [63,64]. The range of the basis is controlled by the oscillator length (b) and the parameter γ [64]. We have used $b=1.6$ fm and $\gamma=2$ fm$^{-1/2}$, although this choice is not critical since the computed observables must be independent of this choice if the basis is chosen large enough. The size of the basis is determined by the number of oscillator functions (N), the maximum excitation energy ($\varepsilon_{\mathrm{max}}$), and the maximum orbital angular momentum for the core-valence motion (ℓ_{max}). In the present calculations we used $N=25$, $\varepsilon_{\mathrm{max}}=35$ MeV, and $\ell_{\mathrm{max}}=3$. Convergence of elastic scattering and breakup cross sections were ensured by using a large enough model space. The CDCC calculations require also the proton + target and ^{7}Be + target optical potentials. For $^{7}\mathrm{Be}+^{208}\mathrm{Pb}$, we used the systematic single-folding potential of Ref. [51] evaluated at 208 MeV (7/8 of the incident energy) whereas for $p+^{208}$Pb the systematic global potential of Koning and Delaroche [65], evaluated at 29.8 MeV (1/8 of the incident energy), was used. The projectile-target coupling potentials were generated with the code THOx [66] and the coupled equations were solved with the code FRESCO [50].

The calculated elastic cross section is shown in Fig. 4. To highlight the effect of the coupling to the breakup channels, the single-channel calculation resulting from the omission of the continuum states in the CDCC calculation is also

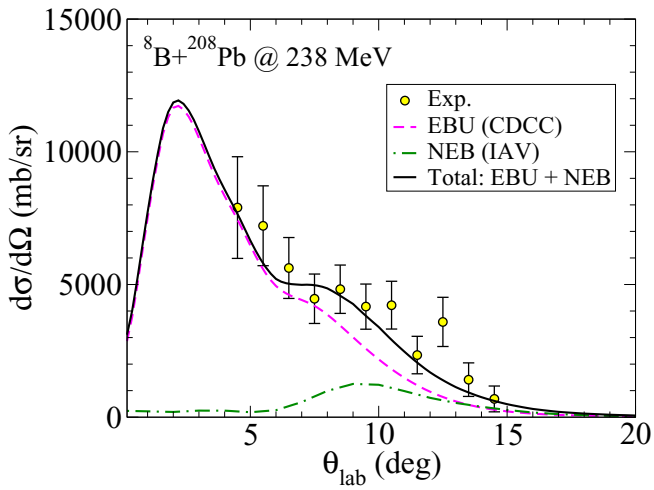

FIG. 5. Experimental ^{7}Be angular distributions from the $^{8}\mathrm{B}+^{208}\mathrm{Pb}$ reaction at $E_{\mathrm{lab}} = 238$ MeV (yellow circle) and comparisons with calculations. Error bars are statistical only.

included (dotted line). The inclusion of the breakup channels reduces the Fresnel peak and slightly increases the cross section at larger angles. These two effects are in the direction of improving the agreement with the data, although some overestimation of the Fresnel peak is still visible.

In addition to the elastically scattered ^{8}B projectile, the present experiment allowed for a clear identification of the produced ^{7}Be fragments, presumably stemming from the breakup and transfer processes. Breakup cross sections are very sensitive to the projectile structure and can be used to investigate the interplay between nuclear structure and reaction dynamics. Therefore, in the following, we analyzed this channel in detail and compared it with the calculations. The angular distribution of these ^{7}Be fragments has been extracted and compared in Fig. 5 with the CDCC prediction. The latter was computed by a suitable transformation of the CDCC breakup amplitudes, using the formalism of Ref. [67]. Besides the systematic potential for $^{7}\mathrm{Be}+^{208}\mathrm{Pb}$ [51] used in this calculation, another two different potentials, namely, the complex Woods-Saxon potential [68] from the fitting of $^{7}\mathrm{Be}+^{208}\mathrm{Pb}$ data in this experiment and Cook's optical model potential [69], were also tested. The calculated breakup cross sections barely showed any difference, indicating that this observable is weakly sensitive to the choice of this potential even for this relatively high energy. From Fig. 5, it is seen that the CDCC calculation reproduces very well the measured distribution (within error bars) up to a scattering angle of $\approx 7^{\circ}$, but underestimates the data at larger angles. At this stage, it is worth recalling that the CDCC method provides only the so-called elastic breakup (EBU) cross section, in which the projectile dissociates while the target remains in its ground state. Since the present experiment is inclusive with respect to the removed proton, other processes can in principle contribute to the ^{7}Be production, in which the proton interacts nonelastically with the target nucleus. These contributions, that we denote globally as nonelastic breakup (NEB), can be efficiently computed with the model proposed by Ichimura, Austern, Vincent (IAV) [70]. The IAV model has been recently revisited by several groups [71–77]. The model has been successfully applied to weakly bound projectiles induced reactions, such as for the exotic ^{11}Be projectile on ^{208}Pb target [39]. The same potentials used in the CDCC calculation were also adopted in the NEB calculation. The results of the NEB calculations are also shown in Fig. 5. The NEB distribution peaks at larger angles as compared to the EBU distribution. When the NEB contribution is added to the EBU, a rather good agreement with the data is obtained (solid line in Fig. 5). Thus, from the present analysis, we conclude that most of the inclusive ^{7}Be yield can be explained as due to an elastic dissociation mechanism, but with a small but not negligible contribution due to nonelastic breakup processes. The breakup angular distribution of $^{11}\mathrm{Be} \rightarrow {}^{10}\mathrm{Be}+n$ on a ^{208}Pb target at 3.5 times the Coulomb barrier has also been recently measured [39]. The integrated breakup cross section of ^{8}B in the present work (779 mb) is approximately only one fourth of that for ^{11}Be (3632 mb). Considering that the proton separation energy of ^{8}B ($S_p = 0.136$ MeV) is much smaller than the neutron separation energy of ^{11}Be ($S_n = 0.502$ MeV), the obtained smaller integrated cross section indicates that the Coulomb and centrifugal barriers experienced by the valence proton in the ground state of ^{8}B may suppress the breakup probability. This interpretation is supported by the study of Ref. [40], where calculations are presented for ^{8}B-induced reactions in which the valence proton is replaced by a neutron, resulting in a much larger cross section, similar to a neutron in ^{11}Be at similar binding energy.

IV. SUMMARY

In summary, new data were presented for the elastic scattering and breakup reactions of ^{8}B on a ^{208}Pb target at an incident energy of $E_{\mathrm{lab}} = 238$ MeV, which corresponds to four times the Coulomb barrier. The elastic scattering angular distribution, which is well reproduced by optical model and CDCC calculations, exhibits the typical Coulomb nuclear interference peak. This is at variance with the case of the neutron-rich halo nucleus ^{11}Be on the same target and at a similar energy [39], where a strong suppression of this interference peak was observed. The extracted reduced total reaction cross section for $^{8}\mathrm{B}+^{208}\mathrm{Pb}$ is similar to that of the $^{7}\mathrm{Be}+^{208}\mathrm{Pb}$ reaction. The present work indicates that the breakup couplings effects, in the elastic scattering for the $^{8}\mathrm{B}+^{208}\mathrm{Pb}$ system at higher energies, do not play an important role. In contrast, a strong suppression in the $^{8}\mathrm{B}+^{208}\mathrm{Pb}$ elastic scattering at energies close to the Coulomb barrier was observed, though the data were rather poorly described by CDCC calculations [30]. This might corroborate the idea of the gradual decreasing of the breakup couplings effects in the elastic scattering for the $^{8}\mathrm{B}+^{208}\mathrm{Pb}$ system. However, to better investigate this issue, further data on elastic scattering and breakup for this system at different energies would be very welcome.

The angular distribution of ^{7}Be fragments was measured for the first time at this energy. The extracted ^{7}Be cross section could be mostly accounted for by the CDCC calculations, thereby indicating the dominance of the EBU mechanism.

To estimate the contribution coming from NEB, additional calculations were performed using the IAV model [70]. The NEB contribution was found to be relevant at angles around the grazing angle. The combined EBU + NEB result describes very well the shape and magnitude of the data.

ACKNOWLEDGMENTS

We would like to acknowledge the staff of HIRFL for the operation of the cyclotron and their friendly collaboration. This work was financially supported by the National Key R&D Program of China (Grant No. 2018YFA0404403), the National Natural Science Foundation of China (Grants No. 11947203, No. 11775013, No. 11575256, and No. U1632138), and the Youth Innovation Promotion Association CAS (No. 2020411). V.G. and J.C.Z. would like to thank the São Paulo Research Foundation (FAPESP) (Grants No. 2016/17612-7 and No. 2018/04965-4) for the financial support. A.M.M. is supported by the Spanish Ministerio de Ciencia, Innovación y Universidades (including FEDER funds) under project FIS2017-88410-P and by the European Union's Horizon 2020 research and innovation program under Grant Agreement No. 654002.

[1] L. F. Canto, P. R. S. Gomes, R. Donangelo, and M. S. Hussein, Phys. Rep. **424**, 1 (2006).
[2] N. Keeley, K. W. Kemper, and K. Rusek, Eur. Phys. J. A **50**, 145 (2014).
[3] J. Kolata, V. Guimarães, and E. Aguilera, Eur. Phys. J. A **52**, 123 (2016).
[4] C. E. Thorn, M. J. LeVine, J. J. Kolata, C. Flaum, P. D. Bond, and J. C. Sens, Phys. Rev. Lett. **38**, 384 (1977).
[5] R. S. Mackintosh, Y. Hirabayashi, and S. Ohkubo, Phys. Rev. C **91**, 024616 (2015).
[6] L. M. Fonseca, R. Linares, V. A. B. Zagatto, F. Cappuzzello, D. Carbone, M. Cavallaro, C. Agodi, J. Lubian, and J. R. B. Oliveira, Phys. Rev. C **100**, 014604 (2019).
[7] L. F. Canto, V. Guimarães, J. Lubián, and M. S. Hussein, Eur. Phys. J. A **56**, 281 (2020).
[8] J. P. Fernández-García *et al.*, Phys. Rev. C **92**, 044608 (2015).
[9] M. Cubero *et al.*, Phys. Rev. Lett. **109**, 262701 (2012).
[10] A. Di Pietro *et al.*, Phys. Rev. Lett. **105**, 022701 (2010).
[11] A. Di Pietro *et al.*, EPJ Web Conf. **66**, 03023 (2014).
[12] P. A. DeYoung *et al.*, Phys. Rev. C **71**, 051601(R) (2005).
[13] L. Acosta *et al.*, Phys. Rev. C **84**, 044604 (2011).
[14] A. Lemasson *et al.*, Phys. Rev. Lett. **103**, 232701 (2009).
[15] A. Lemasson *et al.*, Phys. Rev. C **82**, 044617 (2010).
[16] I. Martel, N. Keeley, K. W. Kemper, and K. Rusek, Phys. Rev. C **102**, 034609 (2020).
[17] N. Keeley, N. Alamanos, K. Kemper, and K. Rusek, Prog. Part. Nucl. Phys. **63**, 396 (2009).
[18] B. B. Back, H. Esbensen, C. L. Jiang, and K. E. Rehm, Rev. Mod. Phys. **86**, 317 (2014).
[19] L. F. Canto, P. R. S. Gomes, R. Donangelo, J. Lubian, and M. S. Hussein, Phys. Rep. **596**, 1 (2015).
[20] T. Motobayashi *et al.*, Phys. Rev. Lett. **73**, 2680 (1994).
[21] T. Kikuchi *et al.*, Phys. Lett. B **391**, 261 (1997).
[22] E. G. Adelberger *et al.*, Rev. Mod. Phys. **83**, 195 (2011).
[23] I. Tanihata, T. Kobayashi, O. Yamakawa, S. Shimoura, K. Ekuni, K. Sugimoto, N. Takahashi, T. Shimoda, and H. Sato, Phys. Lett. B **206**, 592 (1988).
[24] C.W. De Jager, H. De Vries, and C. De Vries, At. Data Nucl. Data Tables **14**, 479 (1974).
[25] G. A. Korolev *et al.*, Phys. Lett. B **780**, 200 (2018).
[26] A. Barioni, J. C. Zamora, V. Guimarães, B. Paes, J. Lubian, E. F. Aguilera, J. J. Kolata, A. L. Roberts, F. D. Becchetti, A. Villano, M. Ojaruega, and H. Jiang, Phys. Rev. C **84**, 014603 (2011).
[27] V. Morcelle *et al.*, Phys. Rev. C **95**, 014615 (2017).
[28] E. F. Aguilera, E. Martinez-Quiroz, D. Lizcano, A. Gómez-Camacho, J. J. Kolata, L. O. Lamm, V. Guimarães, R. Lichtenthäler, O. Camargo, F. D. Becchetti, H. Jiang, P. A. DeYoung, P. J. Mears, and T. L. Belyaeva, Phys. Rev. C **79**, 021601(R) (2009).
[29] J. Lubian, T. Correa, E. F. Aguilera, L. F. Canto, A. Gomez-Camacho, E. M. Quiroz, and P. R. S. Gomes, Phys. Rev. C **79**, 064605 (2009).
[30] M. Mazzocco *et al.*, Phys. Rev. C **100**, 024602 (2019).
[31] V. Guimarães, J. J. Kolata, D. Peterson, P. Santi, R. H. White-Stevens, S. M. Vincent, F. D. Becchetti, M. Y. Lee, T. W. O'Donnell, D. A. Roberts, and J. A. Zimmerman, Phys. Rev. Lett. **84**, 1862 (2000).
[32] J. J. Kolata, V. Guimarães, D. Peterson, P. Santi, R. H. White-Stevens, S. M. Vincent, F. D. Becchetti, M. Y. Lee, T. W. O'Donnell, D. A. Roberts, and J. A. Zimmerman, Phys. Rev. C **63**, 024616 (2001).
[33] J. A. Tostevin, F. M. Nunes, and I. J. Thompson, Phys. Rev. C **63**, 024617 (2001).
[34] N. C. Summers and F. M. Nunes, J. Phys. G: Nucl. Part. Phys. **31**, 1437 (2005).
[35] T. L. Belyaeva, E. F. Aguilera, E. Martinez-Quiroz, A. M. Moro, and J. J. Kolata, Phys. Rev. C **80**, 064617 (2009).
[36] A. Pakou *et al.*, Phys. Rev. C **102**, 031601(R) (2020).
[37] Y. Y. Yang *et al.*, Phys. Rev. C **87**, 044613 (2013).
[38] Y. Y. Yang *et al.*, Phys. Rev. C **98**, 044608 (2018).
[39] F. F. Duan, Y. Y. Yang *et al.*, Phys. Lett. B **811**, 135942 (2020).
[40] R. Kumar and A. Bonaccorso, Phys. Rev. C **84**, 014613 (2011).
[41] Y. Y. Yang, X. Liu, and D. Y. Pang, Phys. Rev. C **94**, 034614 (2016).
[42] J. W. Xia *et al.*, Nucl. Instrum. Methods Phys. Res., Sect. A **488**, 11 (2002).
[43] W. L. Zhan *et al.*, Nucl. Phys. A **805**, 533c (2008).
[44] W. L. Zhan *et al.*, Sci. China Seri. A Math. **42**, 528 (1999).
[45] Z. Y. Sun, W. L. Zhan, Z. Y. Guo, G. Q. Xiao, and J. X. Li, Nucl. Instrum. Methods Phys. Res., Sect. A **503**, 496 (2003).
[46] Y. Y. Yang *et al.*, Nucl. Instrum. Methods Phys. Res., Sect. A **701**, 1 (2013).
[47] Y. Y. Yang *et al.*, Phys. Rev. C **90**, 014606 (2014).
[48] F. F. Duan, Y. Y. Yang *et al.*, Nucl. Sci. Technol. **29**, 165 (2018).
[49] F. F. Duan, Y. Y. Yang *et al.*, Chin. Phys. C **44**, 024001 (2020).
[50] I. J. Thompson, Comput. Phys. Rep. **7**, 167 (1988).
[51] Y. P. Xu and D. Y. Pang, Phys. Rev. C **87**, 044605 (2013).
[52] B. A. Brown, Phys. Rev. C **58**, 220 (1998).
[53] J. J. Kolata and E. F. Aguilera, Phys. Rev. C **79**, 027603 (2009).
[54] H. Esbensen and G. F. Bertsch, Nucl. Phys. A **600**, 37 (1996).

[55] L. Trache, F. Carstoiu, C. A. Gagliardi, and R. E. Tribble, Phys. Rev. Lett. **87**, 271102 (2001).
[56] K. Ogata, S. Hashimoto, Y. Iseri, M. Kamimura, and M. Yahiro, Phys. Rev. C **73**, 024605 (2006).
[57] G. Tabacaru, A. Azhari, J. Brinkley, V. Burjan, F. Carstoiu, C. Fu, C. A. Gagliardi, V. Kroha, A. M. Mukhamedzhanov, X. Tang, L. Trache, R. E. Tribble, and S. Zhou, Phys. Rev. C **73**, 025808 (2006).
[58] S. B. Igamov and R. Yarmukhamedov, Phys. At. Nucl. **71**, 1740 (2008).
[59] O. R. Tojiboev, R. Yarmukhamedov, S. V. Artemov, and S. B. Sakuta, Phys. Rev. C **94**, 054616 (2016).
[60] P. Descouvemont, Phys. Rev. C **70**, 065802 (2004).
[61] J. Huang, C. Bertulani, and V. Guimarães, At. Data Nucl. Data Tables **96**, 824 (2010).
[62] K. M. Nollett and R. B. Wiringa, Phys. Rev. C **83**, 041001(R) (2011).
[63] S. Karataglidis, K. Amos, and B. G. Giraud, Phys. Rev. C **71**, 064601 (2005).
[64] J. A. Lay, A. M. Moro, J. M. Arias, and J. Gómez-Camacho, Phys. Rev. C **85**, 054618 (2012).
[65] A. Koning and J. Delaroche, Nucl. Phys. A **713**, 231 (2003).
[66] R. de Diego, J. M. Arias, J. A. Lay, and A. M. Moro, Phys. Rev. C **89**, 064609 (2014).
[67] R. de Diego, R. Crespo, and A. M. Moro, Phys. Rev. C **95**, 044611 (2017).
[68] C. L. Woods, B. A. Brown, and N. A. Jelley, J. Phys. G **8**, 1699 (1982).
[69] J. Cook, Nucl. Phys. A **388**, 153 (1982).
[70] M. Ichimura, N. Austern, and C. M. Vincent, Phys. Rev. C **32**, 431 (1985).
[71] J. Lei and A. M. Moro, Phys. Rev. C **92**, 044616 (2015).
[72] J. Lei and A. M. Moro, Phys. Rev. C **92**, 061602(R) (2015).
[73] J. Lei, Phys. Rev. C **97**, 034628 (2018).
[74] J. Lei and A. M. Moro, Phys. Rev. C **97**, 011601(R) (2018).
[75] B. V. Carlson, R. Capote, and M. Sin, Few-Body Syst. **57**, 307 (2016).
[76] G. Potel, F. M. Nunes, and I. J. Thompson, Phys. Rev. C **92**, 034611 (2015).
[77] G. Potel, G. Perdikakis, B. V. Carlson, M. C. Atkinson, W. H. Dickhoff, J. E. Escher, M. S. Hussein, J. Lei, W. Li, A. O. Macchiavelli, A. M. Moro, F. M. Nunes, S. D. Pain, and J. Rotureau, Eur. Phys. J. A **53**, 178 (2017).